Science of the Total Environment 898 (2023) 165303

Contents lists available at ScienceDirect

Science of the Total Environment

journal homepage: www.elsevier.com/locate/scitotenv

Reduced atmospheric sulfate enhances fine particulate nitrate formation in eastern China

Liang Wen [a,1], Likun Xue [a,*], Can Dong [a], Xinfeng Wang [a], Tianshu Chen [a], Ying Jiang [a], Rongrong Gu [a], Penggang Zheng [a], Hongyong Li [a], Ye Shan [a], Yujiao Zhu [a], Yong Zhao [b], Xiangkun Yin [b], Hengde Liu [b], Jian Gao [c], Zhijun Wu [d], Tao Wang [e], Hartmut Herrmann [f,g], Wenxing Wang [a]

[a] Environment Research Institute, Shandong University, Qingdao, Shandong 266237, China
[b] Taishan National Reference Climatological Station, Tai'an, Shandong 271000, China
[c] Chinese Research Academy of Environmental Sciences, Beijing 100012, China
[d] State Key Joint Laboratory of Environmental Simulation and Pollution Control, College of Environmental Sciences and Engineering, Peking University, Beijing 100871, China
[e] Department of Civil and Environmental Engineering, Hong Kong Polytechnic University, 99907, Hong Kong
[f] Atmospheric Chemistry Department (ACD), Leibniz Institute for Tropospheric Research (TROPOS), Permoserstraße 15, Leipzig 04318, Germany
[g] School of Environmental Science and Engineering, Shandong University, Qingdao, Shandong 266237, China

ARTICLE INFO

Editor: Jianmin Chen

Keywords:
Nitrate
Sulfate
$PM_{2.5}$
Long-term variation
Mt. Tai
Eastern China

ABSTRACT

Nitrate (NO_3^-) is a major component of atmospheric fine particles. Recent studies in eastern China have shown the increasing trend of NO_3^- in contrast to the ongoing control of nitrogen oxide (NO_x). Here, we elucidate the effects of reduced sulfur dioxide (SO_2) on the enhancement of NO_3^- formation based on field measurements at the summit of Mt. Tai (1534 m a.s.l.) and present detailed modelling analyses. From 2007 to 2018, the measured springtime concentrations of various primary pollutants and fine sulfate (SO_4^{2-}) decreased sharply (−16.4 % to −89.7 %), whereas fine NO_3^- concentration increased by 22.8 %. The elevated NO_3^- levels cannot be explained by the changes in meteorological conditions or other related parameters but were primarily attributed to the considerable reduction in SO_4^{2-} concentrations (−73.4 %). Results from a multi-phase chemical box model indicated that the reduced SO_4^{2-} levels decreased the aerosol acidity and prompted the partitioning of HNO_3 into the aerosol phase. WRF-Chem model analyses suggest that such a negative effect is a regional phenomenon throughout the planetary boundary layer over eastern China in spring. This study provides new insights into the worsening situation of NO_3^- aerosol pollution and has important implications for controlling haze pollution in China.

1. Introduction

Nitrate (NO_3^-) is a major component of atmospheric particles and contributes markedly to aerosol's effects on air quality, climate, and human health (Xie et al., 2016; Xu and Penner, 2012). Over the past decade, severe haze pollution has prompted the Chinese government to implement unprecedentedly stringent air pollution control measures, resulting in considerable reductions in $PM_{2.5}$ concentrations (and many other primary pollutants) and changes in its chemical compositions (Fan et al., 2020). A major change in the aerosol composition was the persistent decrease in sulfate (SO_4^{2-}) concentrations with increasing contributions of NO_3^- to $PM_{2.5}$ in several polluted regions (Wang et al., 2022; Wang et al., 2013; Wen et al., 2018; Zong et al., 2022). Although the decrease in SO_4^{2-} can be explained by the substantial reduction in anthropogenic emissions of sulfur dioxide (SO_2) since 2006 (Liu et al., 2018), the increasing NO_3^- was not in accord with the variations in nitrogen oxide (NO_x) emissions, which showed a downward trend after 2011 (Vasilakos et al., 2018; Wen et al., 2018). Therefore, it is important to consider why NO_3^- pollution worsened against decreasing NO_x emissions to refine the scientific understandings of the complex

* Corresponding author.
E-mail address: xuelikun@sdu.edu.cn (L. Xue).
[1] Now at: Chinese Research Academy of Environmental Sciences, Beijing 100012, China.

https://doi.org/10.1016/j.scitotenv.2023.165303
Received 10 May 2023; Received in revised form 1 July 2023; Accepted 1 July 2023
Available online 5 July 2023

atmospheric chemistry and the control policy for air pollution in China.

Nitrate is chemically produced via the photochemical formation of nitric acid (HNO_3) followed by partitioning into the aerosol phase during sunlight hours, and via the heterogeneous hydrolysis of dinitrogen pentoxide (N_2O_5) on the aerosol surface under dark conditions (Baasandorj et al., 2017; Herrmann et al., 2010; Song and Carmichael, 2001; Wen et al., 2018; Xue et al., 2014a). Although the chemical pathways are relatively well recognized, the NO_3^- formation mechanism in the ambient atmosphere is complex and depends on various chemical and physical factors. NO_x is the parent precursor and essentially drives the NO_3^- formation. Atmospheric oxidants such as the hydroxyl radical (OH) and ozone (O_3) determine the oxidation of NO_x to HNO_3 and N_2O_5 and thus regulate NO_3^- formation (Wang et al., 2009; Wen et al., 2014; Wen et al., 2018). Volatile organic compounds (VOCs) are essential O_3 precursors and indirectly influence NO_3^- production (Sun et al., 2016; Wen et al., 2014; Xue et al., 2014b). Ammonia (NH_3) and other alkaline compounds can alter the aerosol acidity, which regulates the gas-to-particle partitioning of HNO_3 and also affects N_2O_5 hydrolysis (Chen et al., 2016; Guo et al., 2018; Pathak et al., 2009; Paulot et al., 2016; Petetin et al., 2016; Yao and Zhang, 2012). Sulfate formation can also affect NO_3^- production, either by competing with the oxidation of NO_x or modulating the aerosol acidity (Dovrou et al., 2019; He et al., 2012; Xue et al., 2011). In addition, meteorological conditions (e.g., temperature and relative humidity [RH]) also modulate NO_3^- formation and shape the tempo-spatial variations of NO_3^- pollution in the ambient air (Wang et al., 2009). Previous studies have assessed the contributions of anthropogenic NO_x emissions, atmospheric oxidants, NH_3, and meteorological parameters to the NO_3^- pollution in China (Fu et al., 2020; Guo et al., 2018; Pusede et al., 2016; Wen et al., 2018); however, little is known regarding the impact of the primarily reduced SO_2 and SO_4^{2-}, the most outstanding change in the atmospheric environment of China, on the variation trends in NO_3^- formation.

Eastern China has been a hot spot for air pollution in recent decades due to its dense population and fast-paced urbanization. Recent studies have demonstrated the worsening situation of fine particulate NO_3^-, which has overwhelmed SO_4^{2-} to become the dominant secondary ionic compound in $PM_{2.5}$ over this region (Fu et al., 2020; Li et al., 2018); however, the reasons for the increase in NO_3^- have not been fully elucidated. In the present study, we investigate the significant promotion effect of reduced SO_4^{2-} (or SO_2 emissions) on the NO_3^- formation in the regional atmosphere of eastern China, based on field observations at Mt. Tai (a regional background station) coupled with detailed chemical modelling analyses. Our results underline the seesaw effect between sulfate and nitrate in the formation of complex regional air pollution and provide recommendations for the future control of secondary aerosol pollution in China and other countries with similar air quality problems.

2. Experiment and methods

2.1. Measurement site

Intensive field observations were conducted at the Mt. Tai Regional Background Atmospheric Station during the spring (5 March–8 April) of 2018. The station is located on the summit of Mt. Tai (36.16°N, 117.60°E, 1534 a.s.l.), the highest mountain in the center of the North China Plain (NCP; see Fig. 1), and lies alternatively in the upper planetary boundary layer (PBL) or the lower free troposphere. It is operated continuously by Shandong University to record the long-term variations of key trace gases and aerosols in the regional atmosphere of NCP (Sun et al., 2016; Wen et al., 2018) and to elucidate the chemical and physical processes underlying the regional air pollution (Jiang et al., 2020; Zhang et al., 2021; Zhu et al., 2020). To derive the long-term variations in the chemical components of $PM_{2.5}$ and trace gases, the previous measurement data obtained at the same site in spring 2007 (21 March–24 April) were analyzed (Zhou et al., 2010).

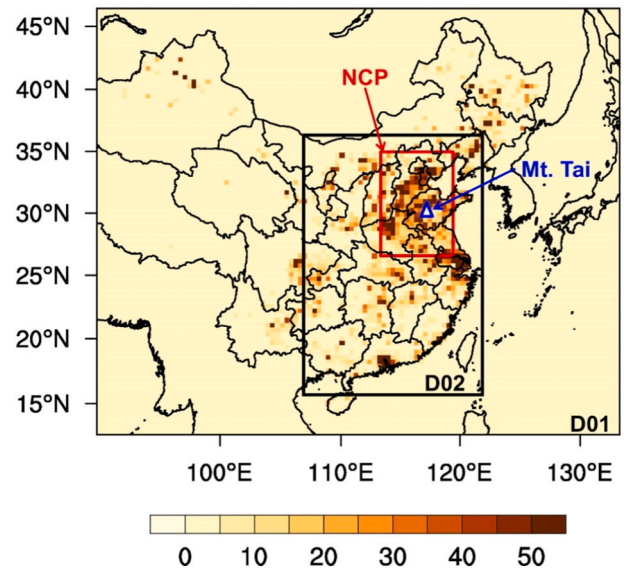

Fig. 1. The WRF-Chem domain settings used in this study. The mother domain (D01) and the nested domain (D02) have a horizontal resolution of 45 and 15 km, respectively. The black and red boxes represent eastern China and the North China Plain (NCP), respectively. The filled contours show the anthropogenic emissions of NO_x (unit in mol km^{-2} h^{-1}) in March 2016 based on the MEIC. The blue triangle denotes the location of the Mt. Tai station.

2.2. Instrument descriptions

An extensive suite of particulate matter properties, gaseous pollutants, and meteorological parameters was detected by several commercial online instruments with strict quality assurance and control procedures (Table S1). During the spring campaign in 2018, the inorganic water-soluble ion concentrations (e.g., Cl^-, NO_3^-, SO_4^{2-}, and NH_4^+) in $PM_{2.5}$ were measured by the online Monitor for AeRosols and GAses (*MARGA; ADI2080, Applikon-ECN, Netherlands*). These particulate ions were collected in a steam jet aerosol collector, and then detected by cationic and anionic ion chromatographs (*ICs; Model 761, Metrohm, Switzerland*) (Brink et al., 2009). The Cl^-, NO_3^-, SO_4^{2-}, and NH_4^+ detection limits were 0.05, 0.05, 0.04, and 0.05 μg m^{-3}, respectively. Previous studies have used MARGA and detailed descriptions of the methods are provided (Shi et al., 2014; Wen et al., 2018; Xie et al., 2015). During the springtime of 2007, the inorganic water-soluble ions in $PM_{2.5}$ were detected by an online ambient ion monitor (*AIM*; *Model URG 9000B, URG Corporation, USA*) operating with the same method (Zhou et al., 2010). The temporal resolution of both MARGA and AIM was 1 h. The ICs were calibrated using standard ion solutions during the campaigns. The $PM_{2.5}$ mass concentrations were detected using a tapered element oscillating microbalance (*Model 1400a, Rupprecht & Patashnick Co., Inc., NY, USA*) in 2007, and using a synchronized hybrid ambient real-time particulate monitor (*Model 5030, Thermo Fisher Scientific, MA, USA*) in 2018. The particle size and counts in a 5 nm–10 μm range were measured using a wide-range particle spectrometer (*Model 1000XP, MSP Corporation, MN, USA*) in 2018.

The NH_3 concentration in the spring of 2018 was detected using MARGA. It was collected in a wet rotating denuder and then analyzed by the ICs. The NO and NO_y (total reactive nitrogen) concentrations in spring 2007 were detected by a chemiluminescence instrument externally equipped with a molybdenum oxide (MoO) catalytic converter (*Models 42cy, Thermo Electron Corporation, MA, USA*). NO_2 was measured by another chemiluminescence analyzer (*Model 42i, Thermo Electron Corporation*) equipped with a blue light converter. In the spring of 2018, the NO_2 monitoring equipment was replaced by a cavity attenuated phase shift spectrometer (*Model T500U, Advanced Pollution Instrumentation Inc., CA, USA*); NO and NO_y were measured using a

Table 1
Statistics of the measured species (Avg. ± SD) in spring 2007 and 2018 on Mt. Tai top. The *t*-test was performed for the differences between the two experiments.

Species	2018	2007	t-test
$PM_{2.5}$ (μg m^{-3})	33.4 ± 25.8	61.5 ± 51.5	$p < 0.01$
NO_3^- (μg m^{-3})	7.0 ± 5.1	5.7 ± 4.7	$p < 0.01$
SO_4^{2-} (μg m^{-3})	3.9 ± 2.8	14.7 ± 10.1	$p < 0.01$
NH_4^+ (μg m^{-3})	2.3 ± 1.8	5.4 ± 3.9	$p < 0.01$
Cl^- (μg m^{-3})	0.7 ± 0.4	0.4 ± 0.4	$p < 0.01$
NH_3 (ppb)	8.4 ± 7.5	——	——
NO (ppb)	0.2 ± 0.3	0.5 ± 0.7	$p < 0.01$
NO_2 (ppb)	1.9 ± 1.7	3.1 ± 2.5	$p < 0.01$
NO_y (ppb)	24.5 ± 17.7	26.5 ± 18.3	$p > 0.05$
O_3 (ppb)	63 ± 14	62 ± 11	$p > 0.05$
SO_2 (ppb)	1.6 ± 1.5	15.5 ± 12.8	$p < 0.01$
CO (ppb)	382 ± 151	457 ± 231	$p < 0.01$
NOR	0.13 ± 0.06	0.11 ± 0.08	$p < 0.01$
$NO_3^-/PM_{2.5}$ (%)	16.8 ± 12.0	11.7 ± 9.0	$p < 0.01$
$SO_4^{2-}/PM_{2.5}$ (%)	12.0 ± 11.4	30.9 ± 18.1	$p < 0.01$
$NH_4^+/PM_{2.5}$ (%)	5.7 ± 4.4	12.2 ± 10.0	$p < 0.01$
$[NO_3^-]/[SO_4^{2-}]$	2.38 ± 1.34	0.61 ± 0.41	$p < 0.01$
Available NH_4^+ (μg m^{-3})	0.6 ± 0.9	−0.3 ± 2.2	$p < 0.01$
Aerosol pH	3.15 ± 0.38	3.01 ± 0.64	$p < 0.01$
T (°C)	3.9 ± 6.4	5.4 ± 4.0	$p < 0.01$
RH (%)	63 ± 27	62 ± 27	$p > 0.05$

Available $NH_4^+ = ([NH_4^+] - 2 * [SO_4^{2-}] - [Cl^-]) * 18$.
NOR (Nitrate Oxidation Ratio) = $[NO_3^-]_s/[NO_y]_s$.
Note that the $[NO_3^-]$, $[NO_y]$, $[NH_4^+]$, $[SO_4^{2-}]$ and $[Cl^-]$ are the molar concentrations of NO_3^-, NO_y, NH_4^+, SO_4^{2-} and Cl^-, respectively. $[NO_3^-]_s$ and $[NO_y]_s$ means the molar concentrations of NO_3^- and NO_y under the standard condition, respectively.
The aerosol pH was calculated using the E-AIM model.

chemiluminescence instrument with an external MoO catalytic converter (*Model T200U, Advanced Pollution Instrumentation Inc.*). The O_3 concentration was detected by an ultraviolet absorption monitor (*Model 49C, Thermo Electron Corporation*) in 2007 and another ultraviolet absorption monitor (*Model T400U, Advanced Pollution Instrumentation Inc.*) in 2018. The SO_2 concentration was measured by an ultraviolet fluorescence analyzer (*Model 43C, Thermo Electron Corporation*) in both campaigns. The CO concentration was detected by infrared absorption analyzer (*Models 300EU and T300U, Advanced Pollution Instrumentation Inc.*) in the two campaigns. These methods and instruments have been widely applied in previous studies, which are described in detail (Sun et al., 2016; Wang et al., 2010; Xue et al., 2014b). The meteorological parameters, including ambient temperature, RH, and wind vector, were provided by the Taishan National Reference Climatological Station.

2.3. Multi-phase chemical box model simulations

A series of simulation experiments were performed using the RACM-CAPRAM multi-phase chemical box model to quantify the effects of particulate sulfate on nitrate formation under light (9:00–15:00 LT) and dark (21:00–3:00 LT) conditions. The model utilizes the Regional Atmospheric Chemistry Mechanism version 2 (RACM2; containing 363 reactions) to simulate gas-phase chemistry (Goliff et al., 2013) and the Chemical Aqueous-Phase RAdical Mechanism version 2.4 (CAPRAM 2.4; including 438 reactions) to simulate liquid-phase processes (Ervens et al., 2003; Herrmann et al., 2000; Herrmann et al., 2005). The gas- and aqueous-phase chemistry was coupled by a phase transfer module (Schwartz, 1986). The most important change in $PM_{2.5}$ components in the last decade was the significant decrease in SO_4^{2-}; therefore, the simulation experiments (Table S2) were run with different initial concentrations of SO_4^{2-} (0–60 μg m^{-3}) and constant concentrations of other species (e.g., NO_2, O_3, and NH_3). The initial NO_2 and O_3 concentrations were set to 25 ppb and 60 ppb, respectively, to match the measured average concentrations of NO_y and O_3 at Mt. Tai. The initial NH_3 concentration was set at 10 ppb, which was close to the sum of the mean gaseous NH_3 and fine particulate NH_4^+ concentrations in the spring of 2018. The initial concentrations of NO, HONO, PAN, and other NO_y species were set to 0. The HCl and Cl^- concentrations were set to 0 to avoid disturbance from $ClNO_2$ formation. The temperature and RH were set at 0 °C and 60 %, respectively, which were similar to the mean values measured at Mt. Tai (Table 1). The liquid water content was set to 1 μmol m^{-3} based on the result of E-AIM thermodynamic model simulation (http://www.aim.env.uea.ac.uk/aim/aim.php) (Clegg et al., 1998). The average particle radius was set to 100 nm depending on the measurement of particle size distribution. The PBL heights were set to 1000 and 500 m for day and night simulations, respectively. Finally, NO_3^- production was simulated based on the prescribed initial conditions and multi-phase atmospheric chemistry schemes in the model.

2.4. Regional model simulations

The regional air quality model WRF-Chem version 3.9.1.1 was used to investigate the impacts of changes in SO_2 emission on the composition of fine particulate matters in eastern China (Grell et al., 2005). The simulation period was from 26 February to 31March, 2018, and the first three days were used for model spin-up. Two domains were applied for the simulations in this study (Fig. 1). Domain 01 (D01) covered East Asia with a horizontal resolution of 45 km, and the nested domain (D02) covered most parts of eastern China with a horizontal resolution of 15 km. The model contained 34 vertical layers with a maximum pressure of 100 hPa. The Moderate-Resolution Imaging Spectroradiometer 30 s terrain and land use data were used. Meteorological initial and boundary conditions were obtained from NCEP global reanalysis data with a resolution of 1° × 1° (available at http://rda.ucar.edu/datasets/ds083.2/, last accessed 12 June 2020). MOZART-4 forecasts were used for chemical initial and boundary conditions (Emmons et al., 2010). The selected physics schemes were Lin microphysics (Lin et al., 1983), RRTMG longwave and shortwave (Iacono et al., 2008), YSU PBL (Hong et al., 2005), and Fast-J photolysis. For chemistry, the CBMZ gas-phase mechanism (Zaveri and Peters, 1999) was used in combination with the MOSAIC 8-bin aerosol module (Zaveri et al., 2008). The MEIC anthropogenic emission inventory comprised 10 primary air pollutants (CO, NO_x, SO_2, VOCs, $PM_{2.5}$, PM_{10}, BC, OC, CO_2, and NH_3) from five sectors (industry, agriculture, power, residential, and transportation). The MEGAN version 2.04 was used for online calculations of biogenic emissions (Guenther et al., 2006). The modelling results from the 15 km domain were used for analysis. Three numerical experiments were performed, which only differed in the input of the anthropogenic

emissions. The base run (2016Emis) used the 2016 MEIC as the anthropogenic emissions; the 2008SO_2 case used the 2016 anthropogenic SO_2 emissions replaced by 2008 anthropogenic SO_2 emissions, and the 2008SO_2NO_x case had the 2016 anthropogenic SO_2 and NO_x emissions replaced by 2008 anthropogenic SO_2 and NO_x emissions, respectively. Simulation results from the base case were validated against the regional air quality measurement data across eastern China (Fig. S1).

3. Result and discussion

3.1. Observed changes in aerosol composition and gaseous pollutants

Table 1 documents the observation results during the two campaigns and shows the large discrepancy in particulate and gaseous pollutants at Mt. Tai between 2007 and 2018. $PM_{2.5}$ concentrations sharply decreased by 45.7 % from 61.5 ± 51.5 μg m^{-3} (mean ± SD) in 2007 to 33.4 ± 25.8 μg m^{-3} in 2018. Simultaneously, SO_2, NO_x and CO levels decreased by 89.7 %, 41.7 % and 16.4 %, respectively. This demonstrates the outstanding achievement of China in reducing primary pollution and improving air quality over the past decade. The ionic composition of $PM_{2.5}$ also changed substantially. SO_4^{2-} concentration decreased by 73.4 % from 14.7 ± 10.1 (2007) to 3.9 ± 2.8 μg m^{-3} (2018), contributing to 38.4 % of the total $PM_{2.5}$ reduction. A substantial decrease of 57.4 % was also found for NH_4^+ concentration. In contrast, the NO_3^- concentration increased by 22.8 % from 5.7 ± 4.7 (2007) to 7.0 ± 5.1 μg m^{-3} (2018). The $NO_3^-/PM_{2.5}$ fraction increased from 11.7 ± 9.0 % (2007) to 16.8 ± 12.0 % (2018), whereas the $SO_4^{2-}/PM_{2.5}$ fraction decreased from 30.9 ± 18.1 % (2007) to 12.0 ± 11.4 % (2018). Consequently, the $[NO_3^-]/[SO_4^{2-}]$ molar ratio sharply increased from 0.61 ± 0.41 in 2007 to 2.38 ± 1.34 in 2018. The enhanced NO_3^- formation was also reflected by the higher nitrogen oxidation ratio (NOR = $[NO_3^-]_s/[NO_y]_s$; the subscript "s" denotes concentration at standard atmospheric conditions) in 2018 (0.13 ± 0.06) than in 2007 (0.11 ± 0.08). Notably, the above-stated differences are statistically significant ($p < 0.01$; Table 1). Fine NO_3^- aerosol increased rapidly and became the dominant secondary ionic species in $PM_{2.5}$. This result generally agrees with the other observation and modelling studies that show the increasing trends of NO_3^- over eastern China (Wang et al., 2013; Wen et al., 2018).

Fig. 2 shows the average diurnal variations in NO_3^-, SO_4^{2-}, $PM_{2.5}$, $NO_3^-/PM_{2.5}$, $SO_4^{2-}/PM_{2.5}$, NO_2, NO_y, SO_2, and O_3 in the spring of 2007 and 2018. All the pollutants exhibited similar diurnal profiles with a broad daytime concentration peak and lower levels at night, indicating the effects of PBL evolution and mountain-valley breezes (Jiang et al., 2020). The SO_2 and SO_4^{2-} concentrations showed systematically

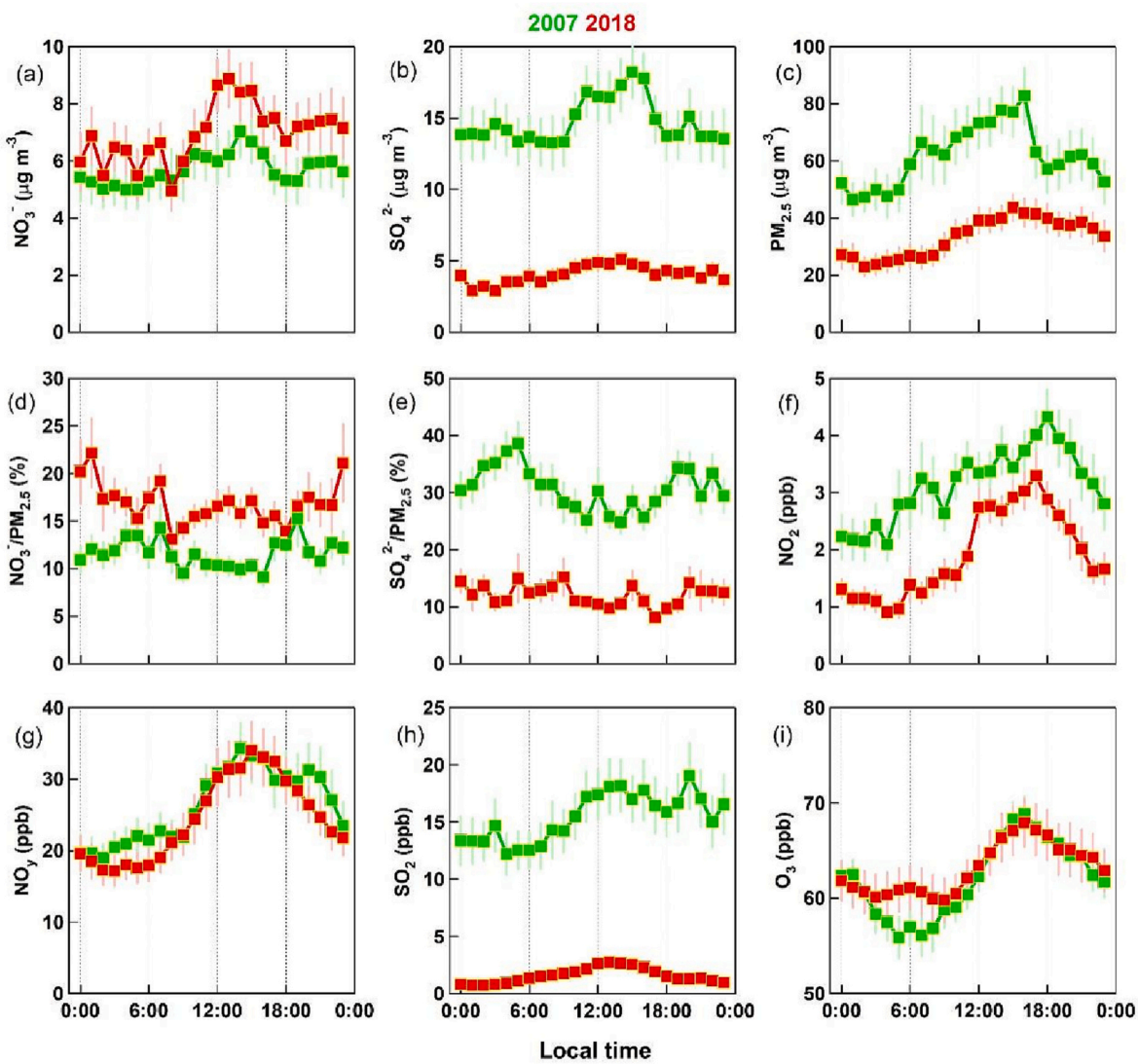

Fig. 2. Average diurnal variations of (a) NO_3^-, (b) SO_4^{2-}, (c) $PM_{2.5}$, (d) $NO_3^-/PM_{2.5}$, (e) $SO_4^{2-}/PM_{2.5}$, (f) NO_2, (g) NO_y, (h) SO_2, and (i) O_3 at the summit of Mt. Tai during the springtime of 2007 (green lines) and 2018 (red lines). The error bar represents the standard error of the mean.

substantial decreases throughout the day from 2007 to 2018. In comparison, the increase in NO_3^- concentrations was higher during the daytime than at night (Fig. 2a). For example, in 2018, NO_3^- showed a rapid build-up during the daytime with an increment (defined as the daytime maximum minus the minimum in the early morning) of 3.5 μg m^{-3}, which was markedly higher than that of 2007 (2.0 μg m^{-3}). An opposite result was derived for SO_4^{2-}, which presented a considerably higher daytime increment in 2007 (5.0 μg m^{-3}) than in 2018 (2.2 μg m^{-3}) (Fig. 2b). This suggests that the atmospheric photochemistry altered to favor the production of NO_3^- rather than SO_4^{2-} in 2018. Notably, the location and elevation of Mt. Tai make it easily affected by the transport of regional air masses (Zhang et al., 2021); therefore, our results should represent air pollution and processes on a regional scale.

3.2. Mechanism of enhanced nitrate formation

To explore the possible reasons for the enhanced NO_3^- formation, the changes in the individual influence factors between spring 2007 and spring 2018 were examined (Table 1). The difference in NO_y levels was insignificant (26.5 ± 18.3 vs. 24.5 ± 17.7 ppbv, $p > 0.05$), whereas the NO_x concentrations were substantially lower in 2018 ($p < 0.01$). Although studies have reported an increasing trend in O_3 (particularly in summer) at Mt. Tai and over eastern China (Ma et al., 2021; Sun et al., 2016), the measured spring O_3 concentrations in the two field campaigns in this work were comparable (62 ± 11 vs. 63 ± 14 ppbv, $p > 0.05$). Thus, the variations in NO_x, NO_y and O_3 (an indicator of atmospheric oxidation intensity) cannot explain the observed NO_3^- enhancement. This differs from the findings in urban areas, such as Beijing, Tangshan, Handan and Shanghai, where nitrate formations were promoted by the enhanced atmospheric oxidation capacity (Fu et al., 2020; Zhou et al., 2022). A metric of available NH_4^+ (available $NH_4^+ = ([NH_4^+] - 2 * [SO_4^{2-}] - [Cl^-]) * 18$) was introduced to quantify the NH_4^+ which can be used to neutralize NO_3^- in $PM_{2.5}$. The value of available NH_4^+ increased from −0.3 ± 2.2 μg m^{-3} in 2007 to 0.6 ± 0.9 μg m^{-3} in 2018, favoring gas-particle partitioning of HNO_3. However, the increase in available NH_4^+ should be attributed to the significant decrease in SO_4^{2-} concentrations rather than the increase in NH_4^+ because the measured NH_4^+ concentration decreased by 57.4 %. The E-AIM simulated aerosol pH value was higher in 2018 (3.15 ± 0.38) than in 2007 (3.01 ± 0.64), suggesting a reduction in aerosol acidity. Air temperature was slightly lower in 2018 (3.9 ± 6.4 °C) than in 2007 (5.4 ± 4.0 °C; $p < 0.01$); however, ambient RH was comparable (62 ± 27 % vs. 63 ± 27 %, $p > 0.05$). Overall, the above examination of the observational data ruled out the possible effects of NO_x, oxidants and RH, and the substantial decline in SO_4^{2-} is the most likely factor leading to the enhanced NO_3^- formation.

Apparent nitrate formation cases were carefully selected to verify the responses of NO_3^- formation to SO_4^{2-} and related parameters. The selection criteria for cases were both observed NO_3^- concentrations and NOR ratios that increased steadily over a long period (i.e., >3 h) with stable weather conditions (i.e., calm or persistent wind direction without wet deposition). A total of four and eight daytime cases as well as three and three nighttime cases were screened out in 2007 and 2018, respectively (Tables 2). Here, we introduced a metric of nitrate conversion rate ($C(NO_3^-) = \frac{[NO_3^-]_{s\ t2} - [NO_3^-]_{s\ t1}}{(t2-t1) * [NO_y]_s}$) to quantify the NO_3^- formation efficiency during each case. Fig. 3 shows that the $C(NO_3^-)$ in 2018 (0.034 ± 0.014 h^{-1} for day cases and 0.049 ± 0.006 h^{-1} for night cases) is markedly higher than those in 2007 (0.024 ± 0.008 and 0.035 ± 0.017 h^{-1} for day and night cases). Correspondingly, the SO_4^{2-} concentrations substantially reduced from 20.8 ± 14.5 (15.6 ± 2.1) μg m^{-3} in 2007 to 4.5 ± 2.6 (4.6 ± 2.1) μg m^{-3} in 2018 during the day (night) cases; the available NH_4^+ concentrations increased from −1.6 ± 2.4 (0.4 ± 2.1) μg m^{-3} to 0.6 ± 0.3 (0.8 ± 1.4) μg m^{-3}. The particulate H^+, which was calculated using the E-AIM model with the observation constraints of aerosol compositions, showed a decreasing variation from 2007 to 2018 (0.41 ± 0.47 vs. 0.23 ± 0.12 μmol m^{-3}). Moreover, the aerosol H^+ concentration presents a positive correlation with SO_4^{2-} concentration (r = 0.37) and a negative relationship with $C(NO_3^-)$ value (r = −0.42; figures not shown). This implies that the reduced SO_4^{2-} enhances NO_3^- production by reducing the aerosol acidity and facilitating the partitioning of HNO_3 into the aerosol phase.

Table 2
Summary of the selected nitrate formation cases with detailed chemical properties in 2007 and 2018 campaigns.

Start moment	Periods (h)	ΔNO_3^- (μg m^{-3})	$P(NO_3^-)$ (μg m^{-3} h^{-1})	$C(NO_3^-)$ (h^{-1})	Avg. NO_2 (ppb)	Avg. NO_y (ppb)	Avg. SO_4^{2-} (μg m^{-3})	Avg. Available NH_4^+ (μg m^{-3})	Avg. O_3 (ppb)	Avg. H^+ (μmol m^{-3})
Day case										
04/04/2007 07:00	7	10.7	1.53	0.032	3.9	17.3	7.0	1.2	56	0.03
04/17/2007 08:00	7	9.2	1.31	0.013	4.6	36.4	40.5	−4.7	68	0.37
04/19/2007 09:00	5	6.2	1.24	0.022	2.2	20.4	22.0	−1.9	66	1.08
04/23/2007 09:00	8	9.4	1.18	0.028	1.8	15.2	13.7	−1.0	68	0.11
03/10/2018 09:00	6	16.5	2.75	0.023	4.2	43.2	5.9	0.7	62	0.17
03/12/2018 08:00	4	7.2	1.80	0.040	2.3	16.3	2.7	0.3	66	0.15
03/13/2018 08:00	4	8.4	2.10	0.032	1.3	23.7	2.9	0.2	69	0.22
03/19/2018 11:00	4	7.6	1.90	0.050	2.4	13.7	4.1	0.9	56	0.16
03/21/2018 16:00	3	7.0	2.33	0.050	3.4	16.8	0.9	0.7	54	0.09
03/23/2018 08:00	5	11.3	2.26	0.044	1.5	18.6	3.6	0.7	62	0.12
03/25/2018 08:00	5	9.6	1.92	0.017	2.8	40.8	8.3	1.1	74	0.28
03/27/2018 07:00	5	7.7	1.54	0.018	1.9	30.9	7.6	0.3	73	0.27
Night case										
03/28/2007 22:00	6	9.9	1.65	0.040	1.3	14.9	17.6	1.1	62	0.13
04/01/2007 00:00	4	8.2	2.05	0.049	2.2	15.1	13.5	−1.9	50	0.08
04/20/2007 20:00	4	5.7	1.43	0.017	6.4	30.3	15.7	2.1	55	1.09
03/24/2018 00:00	4	12.8	3.20	0.051	0.8	22.7	2.8	1.0	62	0.45
03/28/2018 00:00	5	8.0	1.60	0.043	1.4	13.4	4.0	−0.6	65	0.42
03/29/2018 19:00	3	16.9	5.63	0.054	2.4	37.7	6.9	2.1	81	0.25

$\Delta NO_3^- = NO_{3\ t2}^- - NO_{3\ t1}^-$
$P(NO_3^-) = (NO_{3\ t2}^- - NO_{3\ t1}^-) / (t2 - t1)$
$C(NO_3^-) = ([NO_3^-]_{s\ t2} - [NO_3^-]_{s\ t1}) / (t2 - t1) / [Avg.\ NO_y]_s$.
Available $NH_4^+ = ([NH_4^+] - 2 * [SO_4^{2-}] - [Cl^-]) * 18$.
The t2 and t1 represent the ending and beginning moment of a nitrate formation case.
The concentration of H^+ was calculated with the E-AIM model.

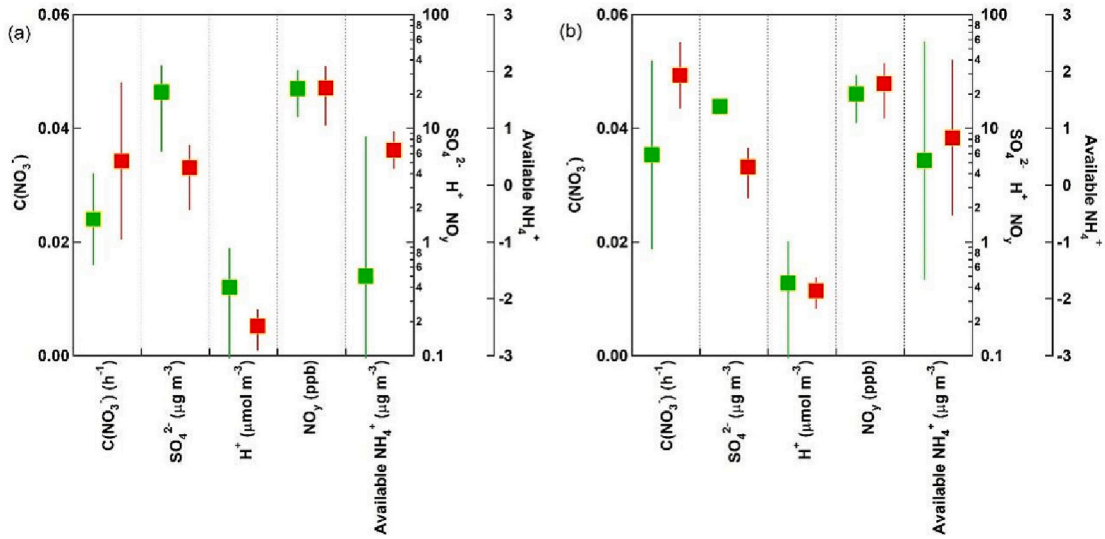

Fig. 3. Comparison of $C(NO_3^-)$, SO_4^{2-}, particulate H^+, NO_y, and available NH_4^+ between the apparent nitrate formation cases during (a) daytime and (b) nighttime in 2007 (green) and 2018 (red). Refer to main context for the criteria for the selection of typical nitrate formation cases. In this study, 8 (4) daytime cases and 3 (3) nighttime cases were selected in 2018 (2007). The error bar represents the standard deviation of the mean.

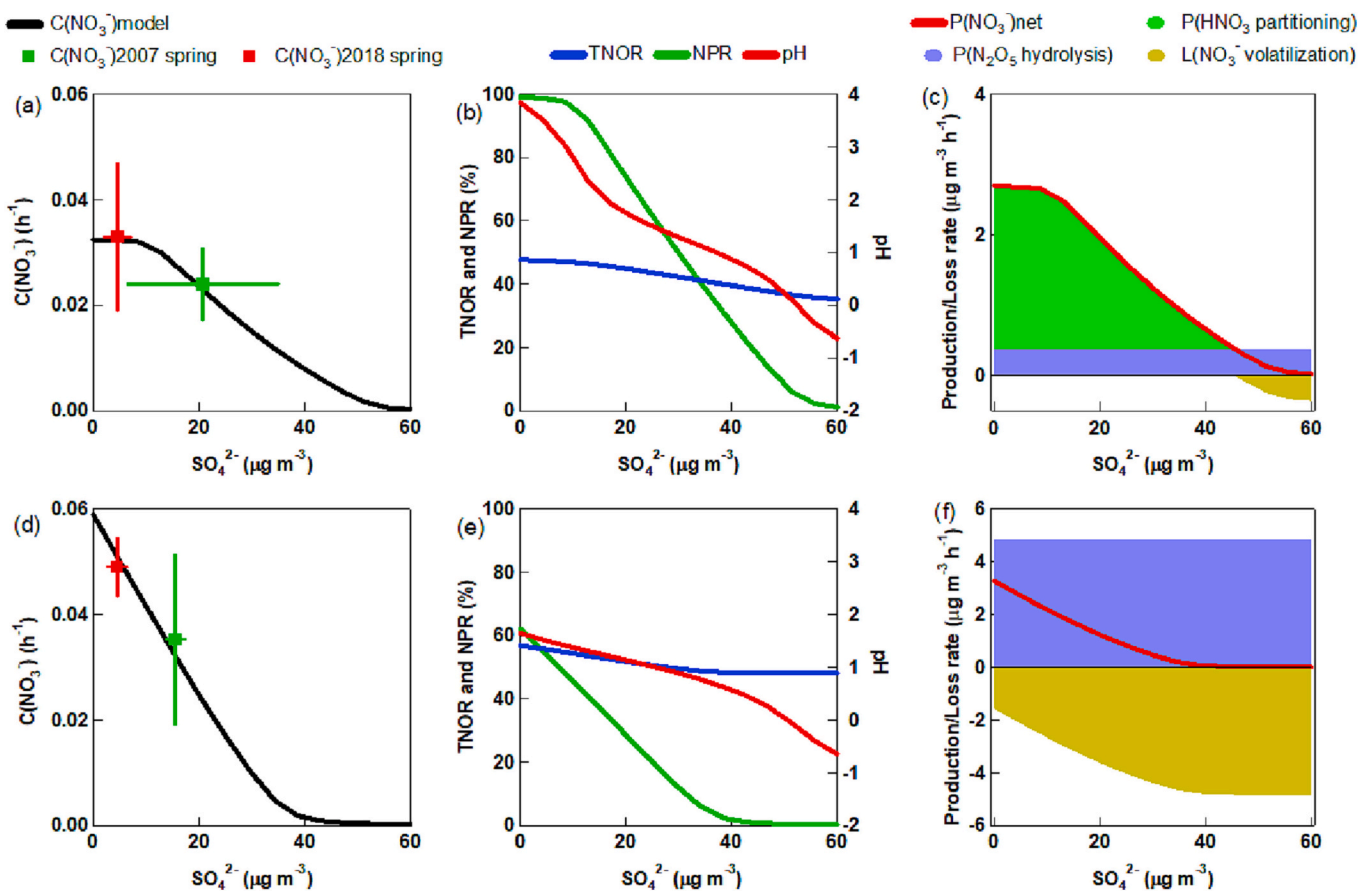

Fig. 4. RACM-CAPRAM simulated results of $C(NO_3^-)$, total nitrate oxidation ratio (TNOR = $([NO_3^-] + [HNO_3])/[NO_y]$), nitrate partitioning ratio (NPR = $[NO_3^-]/([NO_3^-] + [HNO_3])$), pH value, and NO_3^- production budgets based on different SO_4^{2-} inputs in (a–c) sunlight and (d–f) dark scenarios. Quadratic markers (a and d) represent the average $C(NO_3^-)$ vs. average SO_4^{2-} in the screened observation cases at Mt. Tai in 2007 and 2018, where error bars representing the stand deviations.

To further elucidate the mechanism by which SO_4^{2-} affects NO_3^- formation, the RACM-CAPRAM multi-phase chemical box model was deployed to simulate the nitrate production processes under both sunlight and dark conditions. The model was prescribed to the measured average atmospheric conditions at Mt. Tai but with varying initial SO_4^{2-} concentrations (Table S2). Fig. 4 documents the dependence of the model-simulated $C(NO_3^-)$, the total nitrate oxidation ratio (TNOR = $([NO_3^-] + [HNO_3])/[NO_y]$), the nitrate partitioning ratio (NPR = $[NO_3^-]/([NO_3^-] + [HNO_3])$), and the pH value of aerosol liquid water to the different SO_4^{2-} inputs. Several significant findings can be drawn from

the plot. First, the modelled C(NO_3^-) clearly shows a strong negative dependence on the SO_4^{2-} concentrations, which is consistent with the observational results of reduced SO_4^{2-} vs. increased NO_3^- between 2007 and 2018. Furthermore, the measurement-deduced C(NO_3^-) values for the selected cases generally fall on the modelled curves, indicating the applicability of model simulations. Second, the pH value shows a strong negative dependence on the SO_4^{2-} input, illustrating the dominant role of SO_4^{2-} in altering the aerosol acidity under the typical ammonia-rich conditions in the NCP region (note that the sum of NH_3 and NH_4^+ concentrations were fixed in the model simulations) (Wen et al., 2018). Third, the TNOR presents a slight negative relationship with the SO_4^{2-} input, suggesting that the reduced SO_4^{2-} promotes the oxidation of NO_2 to HNO_3 and NO_3^-. In comparison, the NPR shows a considerably stronger negative correlation with SO_4^{2-}, demonstrating the key role of HNO_3 gas-to-particle partitioning in the effect of SO_4^{2-} on the NO_3^- formation. The NPR values decrease from 99 % (sunlight) and 70 % (dark) to 0 %, corresponding to the pH variation from 3.8 (sunlight) and 1.7 (dark) to −0.6, respectively, agreeing with the transition from 0 % to 100 % partitioning of $HNO_{3(g)}$ to particle phase in the pH range of 0–5 at 0 °C by the ISORROPIA-II (Guo et al., 2016). From 2007 to 2018, the average SO_4^{2-} concentrations decreased from 20.8 (15.6) to 4.5 (4.6) μg m^{-3} during the selected daytime (nighttime) nitrate formation cases. After 6 h of oxidation in the model, such reduced SO_4^{2-} levels resulted in increases of 2.8 % (3.7 %) and 26.9 % (15.4 %) of TNOR and NPR under sunlight (dark) conditions, respectively. Therefore, the decreased SO_4^{2-} levels enhanced the NO_3^- formation primarily by reducing the aerosol acidity and promoting the partitioning of HNO_3 into the aerosol phase.

Fig. 4 also shows the chemical budget of NO_3^- as a function of SO_4^{2-} inputs. As expected, the HNO_3 formation and partitioning was the dominant NO_3^- formation pathway during the daytime, whereas the heterogeneous hydrolysis of N_2O_5 predominated at night; volatilization to the gas phase was its main loss pathway. With the decreasing SO_4^{2-} levels, the partitioning of HNO_3 into particles was significantly prompted during the day. However, at night, the decrease in SO_4^{2-} exerted little effect on the heterogeneous hydrolysis reactions of N_2O_5, but reduced the volatilization loss of the formed NO_3^- aerosol.

3.3. Implications for regional nitrate pollution

According to the MEIC (available at http://www.meicmodel.org/, last accessed: 6 January 2021), anthropogenic SO_2 emissions in March had been reduced by 56.9 % over eastern China from 2008 to 2016. Fig. 5 (plot based on the results of the "base" and the "2008SO_2" scenarios) shows the impact of reduced anthropogenic SO_2 emissions on springtime fine particulate sulfate and nitrate concentrations on the regional scale. The model-simulated domain mean SO_4^{2-} concentrations decreased by 53.0 % and 54.0 % at the surface and at 850 hPa (~1500 m above the sea level), respectively, which is comparable to the SO_2 emission reductions. Obviously, the promotion effect of reduced SO_2 (SO_4^{2-}) on nitrate formation is a regional phenomenon, not only at the surface but also aloft. The average domain NO_3^- concentrations at the surface and 850 hPa increased by 16.5 % and 56.3 %, respectively. Notably, the changes in NO_3^- were regionally very inhomogeneous. For example, at 850 hPa, the NCP region, where Mt. Tai is located,

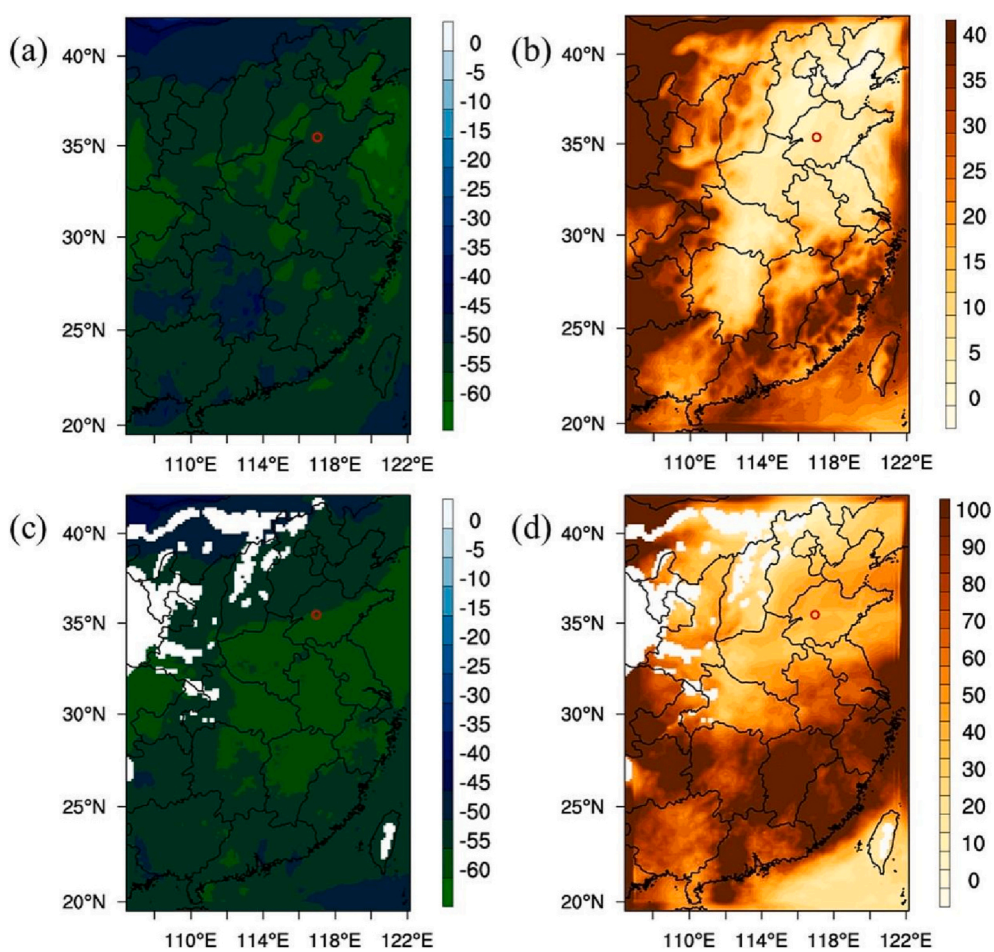

Fig. 5. WRF-Chem simulated percentage changes of (a) SO_4^{2-} (b) NO_3^- at the surface, and (c) SO_4^{2-} (d) NO_3^- at 850 hPa (~1500 m above the sea level). The red circle denotes the location of Mt. Tai. Results from the base scenario (2016Emis) and the scenario with the 2016 anthropogenic SO_2 emissions replaced by 2008 anthropogenic SO_2 emissions (2008SO_2) were used. Percentage change $= \frac{(2016Emis)-(2008SO_2)}{2008SO_2} * 100\%$.

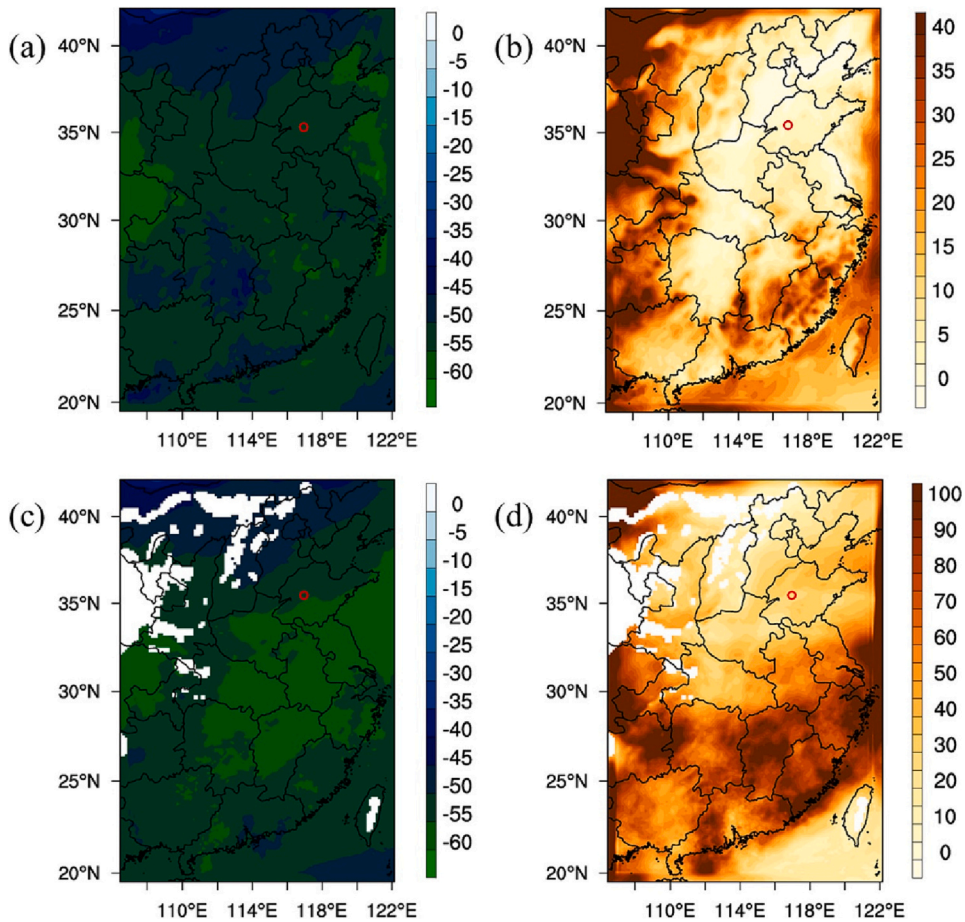

Fig. 6. WRF-Chem simulated percentage changes of (a) SO_4^{2-} and (b) NO_3^- at the surface, and (c) SO_4^{2-} and (d) NO_3^- at 850 hPa (~1500 m above the sea level). The red circles denote the location of Mt. Tai. Results from the base scenario (2016Emis) and the scenario with the respective 2016 anthropogenic SO_2 and NO_x emissions replaced by 2008 anthropogenic SO_2 and NO_x emissions (2008SO_2NO_x) were used. Percentage change $= \frac{(2016Emis)-(2008SO_2NO_x)}{2008SO_2NO_x} * 100\%$.

experienced a relatively lower percentage increase (38.7 %) than other areas. The model-simulated changes in SO_4^{2-} and NO_3^- concentrations at Mt. Tai were −54.8 % and 35.2 %, respectively. The larger increase in NO_3^- concentrations can be explained by the fact that the NO_x emissions were maintained at the 2016 level in the "2008SO_2" scenario. Comparing the base scenario with the "2008SO_2NO_x" case, which had larger NO_x emissions (Fig. S2), the percentage increase in NO_3^- concentrations at Mt. Tai was 24.9 % (Fig. 6), which was substantially closer to the observed value of 22.8 %. Overall, the trends of the modelled impacts of reduced SO_2 emissions on the SO_4^{2-} and NO_3^- concentrations in the NCP were consistent with the observed results at Mt. Tai discussed above.

Over the past decade, China has achieved great success in reducing anthropogenic SO_2 emissions, which has led to significant achievements in reducing concentrations of primary and secondary air pollutants. However, as evidenced by the present study, the largely reduced SO_2 and SO_4^{2-} have enhanced the formation of NO_3^- aerosols in eastern China and weakened the effectiveness of the national NO_x emission control implemented since 2012. This point of view is also supported by results from the WRF-Chem model. From 2008 to 2016, most areas of eastern China experienced considerable reductions in NO_x emissions, and the domain mean NO_x concentrations decreased by 10.6 % (Fig. S2). Fig. 6 shows the differences in SO_4^{2-} and NO_3^- concentrations between the baseline and the "2008SO_2NO_x" scenarios. The concentration of NO_3^- still increased remarkably, although to a lesser extent, with decreasing NO_x emissions.

Overall, this study helps to explain the increasing trend of fine particulate NO_3^- concentrations observed at Mt. Tai and in eastern China as reported by other studies, which expounded the important influencing effects of high NO_x levels, increased atmospheric oxidation capacity and abundant ammonia emissions (Fu et al., 2020; Guo et al., 2018; Li et al., 2018; Wen et al., 2018). Recently, nitrate has become a vital control target to mitigate haze pollution in China. This study has important implications for the future control policy against nitrate aerosol pollution. Considering the complex dependence of NO_3^- formation on the abundances of NO_x, SO_2, O_3 and NH_3 and the projected variation trends of these compounds, more anthropogenic NO_x emission reductions would be the most efficient way to alleviate the worsening situation of nitrate pollution in China.

4. Conclusions

We compared two field measurements of fine particulate nitrate chemistry in the springs of 2007 and 2018 at the summit of Mt. Tai (1534 m a.s.l.), the highest mountain in the center of the NCP region. Compared with the 2007 observations, the measured concentrations of various primary pollutants and fine sulfate in 2018 decreased sharply (ranging from −16.4 % to −89.7 %), whereas the average concentration of NO_3^- increased by 22.8 % (from 5.7 ± 4.7 to 7.0 ± 5.1 μg m^{-3}). The increased NO_3^- concentration was primarily related to the considerable reduction of SO_4^{2-} by −73.4 %, and was less influenced by the meteorological conditions or other parameters. The case analysis and RACM-CAPRAM model simulations suggest that the enhanced nitrate formation was predominately caused by the reduced aerosol acidity and, thus, the gas-particle partitioning of HNO_3 due to decreased sulfate concentration. The WRF-Chem simulations show the consistency of such a

negative effect in the PBL over eastern China during springtime. This study provides new insights into the causes of the worsening nitrate pollution over eastern China and has important implications for the future control of haze pollution.

CRediT authorship contribution statement

Liang Wen: Data curation, Formal analysis, Funding acquisition, Investigation, Software, Roles/Writing-original draft, Writing – review & editing.

Likun Xue: Funding acquisition, Investigation, Project administration Resources, Supervision, Validation, Writing – review & editing.

Can Dong: Formal analysis, Funding acquisition, Investigation, Software, Roles/Writing-original draft, Writing – review & editing.

Xinfeng Wang: Data curation, Validation.
Tianshu Chen: Data curation.
Ying Jiang: Data curation.
Rongrong Gu: Data curation.
Penggang Zheng: Data curation.
Hongyong Li: Data curation.
Ye Shan: Data curation.
Yujiao Zhu: Validation.
Yong Zhao: Data curation.
Xiangkun Yin: Data curation.
Hengde Liu: Data curation.
Jian Gao: Validation.
Zhijun Wu: Validation, Funding acquisition.
Tao Wang: Validation
Hartmut Herrmann: Validation
Wenxing Wang: Validation

Declaration of competing interest

The authors declare that they have no known competing financial interests or personal relationships that could have appeared to influence the work reported in this paper.

Data availability

Data will be made available on request.

Acknowledgement

This study was sponsored by the National Natural Science Foundation of China (42075094 and 41905113), National Key Research and Development Program of China (2022YFC3701101), and special fund of State Key Joint Laboratory of Environmental Simulation and Pollution Control (8102000410). We thank Tsinghua University for providing the MEIC emission inventory, and thank Dr. Yafang Cheng at Max Planck Institute for Chemistry and Dr. Meng Gao at Hong Kong Baptist University for providing the anthropogenic emission processing tools.

Appendix A. Supplementary data

Supplementary data to this article can be found online at https://doi.org/10.1016/j.scitotenv.2023.165303.

References

Baasandorj, M., Hoch, S.W., Bares, R., Lin, J.C., Brown, S.S., Millet, D.B., et al., 2017. Coupling between chemical and meteorological processes under persistent cold-air pool conditions: evolution of wintertime $PM_{2.5}$ pollution events and N_2O_5 observations in Utah's Salt Lake Valley. Environ. Sci. Technol. 51, 5941–5950.
Brink, H., Otjes, R., Jongejan, P., Kos, G., 2009. Monitoring of the ratio of nitrate to sulphate in size-segregated submicron aerosol in the Netherlands. Atmos. Res. 92, 270–276.
Chen, D., Liu, Z., Fast, J., Ban, J., 2016. Simulations of sulfate–nitrate–ammonium (SNA) aerosols during the extreme haze events over northern China in October 2014. Atmos. Chem. Phys. 16, 10707–10724.
Clegg, S.L., Brimblecombe, P., Wexler, A.S., 1998. Thermodynamic model of the system H^+-NH_4^+-Na^+-SO_4^{2-}-NO_3^--Cl^--H_2O at 298.15 K. J. Phys. Chem. 102, 2155–2171.
Dovrou, E., Rivera-Rios, J.C., Bates, K.H., Keutsch, F.N., 2019. Sulfate formation via cloud processing from isoprene hydroxyl hydroperoxides (ISOPOOH). Environ. Sci. Technol. 53, 12476–12484.
Emmons, L.K., Walters, S., Hess, P.G., Lamarque, J.F., Pfister, G.G., Fillmore, D., et al., 2010. Description and evaluation of the Model for Ozone and Related chemical Tracers, version 4 (MOZART-4). Geosci. Model Dev. 3, 43–67.
Ervens, B., George, C., Williams, J.E., Buxton, G.V., Salmon, G.A., Bydder, M., et al., 2003. CAPRAM 2.4 (MODAC mechanism): an extended and condensed tropospheric aqueous phase mechanism and its application. J. Geophys. Res. 108 https://doi.org/10.1029/2002JD002202.
Fan, H., Zhao, C., Yang, Y.A., 2020. Comprehensive analysis of the spatio-temporal variation of urban air pollution in China during 2014–2018. Atmos. Environ. 220, 117066.
Fu, X., Wang, T., Gao, J., Wang, P., Liu, Y., Wang, S., et al., 2020. Persistent heavy winter nitrate pollution driven by increased photochemical oxidants in Northern China. Environ. Sci. Technol. 54, 3881–3889.
Goliff, W.S., Stockwell, W.R., Lawson, C.V., 2013. The regional atmospheric chemistry mechanism, version 2. Atmos. Environ. 68, 174–185.
Grell, G.A., Peckham, S.E., Schmitz, R., McKeen, S.A., Frost, G., Skamarock, W.C., et al., 2005. Fully coupled "online" chemistry within the WRF model. Atmos. Environ. 39, 6957–6975.
Guenther, A., Karl, T., Harley, P., Wiedinmyer, C., Palmer, P.I., Geron, C., 2006. Estimates of global terrestrial isoprene emissions using MEGAN (model of emissions of gases and aerosols from nature). Atmos. Chem. Phys. 6, 3181–3210.
Guo, H., Sullivan, A.P., Campuzano-Jost, P., Schroder, J.C., Lopez-Hilfiker, F.D., Dibb, J. E., et al., 2016. Fine particle pH and the partitioning of nitric acid during winter in the northeastern United States. J. Geophys. Res. A 121, 10355–10376.
Guo, H., Otjes, R., Schlag, P., Kiendler-Scharr, A., Nenes, A., Weber, R.J., 2018. Effectiveness of ammonia reduction on control of fine particle nitrate. Atmos. Chem. Phys. 18, 12241–12256.
He, K., Zhao, Q., Ma, Y., Duan, F., Yang, F., Shi, Z., et al., 2012. Spatial and seasonal variability of $PM_{2.5}$ acidity at two Chinese megacities: insights into the formation of secondary inorganic aerosols. Atmos. Chem. Phys. 12, 1377–1395.
Herrmann, H., Ervens, B., Jacobi, H.W., Wolke, R., Nowacki, P., Zellner, R., 2000. CAPRAM2.3: a chemical aqueous phase radical mechanism for tropospheric chemistry. J. Atmos. Chem. 36, 231–284.
Herrmann, H., Tilgner, A., Barzaghi, P., Majdik, Z., Gligorovski, S., Poulain, L., et al., 2005. Towards a more detailed description of tropospheric aqueous phase organic chemistry: CAPRAM 3.0. Atmos. Environ. 39, 4351–4363.
Herrmann, H., Hoffmann, D., Schaefer, T., Brauer, P., Tilgner, A., 2010. Tropospheric aqueous-phase free-radical chemistry: radical sources, spectra, reaction kinetics and prediction tools. Chemphyschem. 11, 3796–3822.
Hong, S., Noh, Y., Dudhia, J., 2005. A new vertical diffusion package with an explicit treatment of entrainment processes. Mon. Weather Rev. 134, 2318–2341.
Iacono, M.J., Delamere, J.S., Mlawer, E.J., Shephard, M.W., Clough, S.A., Collins, W.D., 2008. Radiative forcing by long-lived greenhouse gases: calculations with the AER radiative transfer models. J. Geophys. Res. 113 https://doi.org/10.1029/2008JD009944.
Jiang, Y., Xue, L.K., Gu, R., Jia, M., Zhang, Y., Wen, L., et al., 2020. Sources of nitrous acid (HONO) in the upper boundary layer and lower free troposphere of the North China Plain: insights from the Mount Tai Observatory. Atmos. Chem. Phys. 20, 12115–12131.
Li, H., Zhang, Q., Zheng, B., Chen, C., Wu, N., Guo, H., et al., 2018. Nitrate-driven urban haze pollution during summertime over the North China Plain. Atmos. Chem. Phys. 18, 5293–5306.
Lin, Y.L., Farley, R.D., Orville, H.D., 1983. Bulk parameterization of the snow field in a cloud model. J. Appl. Meteorol. 22, 1065–1092.
Liu, M., Huang, X., Song, Y., Xu, T., Wang, S., Wu, Z., et al., 2018. Rapid SO_2 emission reductions significantly increase tropospheric ammonia concentrations over the North China Plain. Atmos. Chem. Phys. 18, 1–19.
Ma, X., Huang, J., Zhao, T., Liu, C., Zhao, K., Xing, J., et al., 2021. Rapid increase in summer surface ozone over the North China Plain during 2013–2019: a side effect of particulate matter reduction control? Atmos. Chem. Phys. 21, 1–16.
Pathak, R.K., Wu, S., Wang, T., 2009. Summertime $PM_{2.5}$ ionic species in four major cities of China: nitrate formation in an ammonia-deficient atmosphere. Atmos. Chem. Phys. 9, 1711–1722.
Paulot, F., Ginoux, P., Cooke, W.F., Donner, L.J., Fan, S., Lin, M.Y., et al., 2016. Sensitivity of nitrate aerosols to ammonia emissions and to nitrate chemistry: implications for present and future nitrate optical depth. Atmos. Chem. Phys. 16, 1459–1477.
Petetin, H., Sciare, J., Bressi, M., Gros, V., Rosso, A., Sanchez, O., et al., 2016. Assessing the ammonium nitrate formation regime in the Paris megacity and its representation in the CHIMERE model. Atmos. Chem. Phys. 16, 10419–10440.
Pusede, S.E., Duffey, K.C., Shusterman, A.A., Saleh, A., Laughner, J.L., Wooldridge, P.J., et al., 2016. On the effectiveness of nitrogen oxide reductions as a control over ammonium nitrate aerosol. Atmos. Chem. Phys. 16, 2575–2596.
Schwartz, S.E., 1986. Mass-transport considerations pertinent to aqueous phase reactions of gases in liquid-water clouds. In: Chem. Mul. Atmos. Sys, 6, pp. 415–471.
Shi, Y., Chen, J., Hu, D., Wang, L., Yang, X., Wang, X., 2014. Airborne submicron particulate (PM_1) pollution in Shanghai, China: chemical variability, formation/

dissociation of associated semi-volatile components and the impacts on visibility. Sci. Total Environ. 473-474, 199–206.
Song, C.H., Carmichael, G.R., 2001. Gas-particle partitioning of nitric acid modulated by alkaline aerosol. J. Atmos. Chem. 40, 1–22.
Sun, L., Xue, L.K., Wang, T., Gao, J., Ding, A.J., Cooper, O.R., et al., 2016. Significant increase of summertime ozone at Mount Tai in Central Eastern China. Atmos. Chem. Phys. 16, 10637–10650.
Vasilakos, P., Russell, A., Weber, R., Nenes, A., 2018. Understanding nitrate formation in a world with less sulfate. Atmos. Chem. Phys. 18, 12765–12775.
Wang, J.Q., Gao, J., Che, F., Wang, Y., Lin, P., Zhang, Y., 2022. Decade-long trends in chemical component properties of $PM_{2.5}$ in Beijing, China (2011−2020). Sci. Total Environ. 832, 154664.
Wang, T., Nie, W., Gao, J., Xue, L.K., Gao, X.M., Wang, X.F., et al., 2010. Air quality during the 2008 Beijing Olympics: secondary pollutants and regional impact. Atmos. Chem. Phys. 10, 7603–7615.
Wang, X., Zhang, Y., Chen, H., Yang, X., Chen, J., 2009. Particulate nitrate formation in a highly polluted urban area a case study by single-particle mass spectrometry in Shanghai. Environ. Sci. Technol. 43, 3061–3066.
Wang, Y., Zhang, Q., He, H., Zhang, Q., 2013. Sulfate-nitrate-ammonium aerosols over China: response to 2000–2015 emission changes of sulfur dioxide, nitrogen oxides, and ammonia. Atmos. Chem. Phys. 13, 2635–2652.
Wen, L., Chen, J.M., Yang, L.X., Wang, X.F., Xu, C.H., Sui, X., et al., 2014. Enhanced formation of fine particulate nitrate at a rural site on the North China Plain in summer: the important roles of ammonia and ozone. Atmos. Environ. 101, 294–302.
Wen, L., Xue, L.K., Wang, X.F., Xu, C.H., Chen, T., Yang, L.X., et al., 2018. Summertime fine particulate nitrate pollution in the North China Plain: increasing trends, formation mechanisms and implications for control policy. Atmos. Chem. Phys. 18, 11261–11275.
Xie, Y., Ding, A.J., Nie, W., Mao, H., Qi, X., Huang, X., et al., 2015. Enhanced sulfate formation by nitrogen dioxide: implications from in situ observations at the SORPES station. J. Geophys. Res. 120, 12679–12694.
Xie, Y., Dai, H., Dong, H., Hanaoka, T., Masui, T., 2016. Economic impacts from $PM_{2.5}$ pollution-related health effects in China: a provincial-level analysis. Environ. Sci. Technol. 50, 4836–4843.
Xu, L., Penner, J.E., 2012. Global simulations of nitrate and ammonium aerosols and their radiative effects. Atmos. Chem. Phys. 12, 9479–9504.
Xue, J., Lau, A.K.H., Yu, J.Z., 2011. A study of acidity on $PM_{2.5}$ in Hong Kong using online ionic chemical composition measurements. Atmos. Environ. 45, 7081–7088.
Xue, J., Yuan, Z., Lau, A.K.H., Yu, J.Z., 2014a. Insights into factorsaffectingnitrate in $PM_{2.5}$ inapolluted high NO_x environment through hourly observations and size distribution measurements. J. Geophys. Res. 119, 4888–4902.
Xue, L.K., Wang, T., Gao, J., Ding, A.J., Zhou, X.H., Blake, D.R., et al., 2014b. Ground-level ozone in four Chinese cities: precursors, regional transport and heterogeneous processes. Atmos. Chem. Phys. 14, 13175–13188.
Yao, X.H., Zhang, L., 2012. Supermicron modes of ammonium ions related to fog in rural atmosphere. Atmos. Chem. Phys. 12, 11165–11178.
Zaveri, R.A., Peters, L.K., 1999. A new lumped structure photochemical mechanism for large-scale applications. J. Geophys. Res. A 104, 30387–30415.
Zaveri, R.A., Easter, R.C., Fast, J.D., Peters, L.K., 2008. Model for simulating aerosol interactions and chemistry (MOSAIC). J. Geophys. Res. 113 https://doi.org/10.1029/2007JD008782.
Zhang, Y., Xue, L.K., Li, H., Chen, T., Mu, J., Dong, C., et al., 2021. Source apportionment of regional ozone pollution observed at Mount Tai, North China: application of Lagrangian photochemical trajectory model and implications for control policy. J. Geophys. Res. A 126 doi: e2020JD033519.
Zhou, M., Nie, W., Qiao, L., Huang, D.D., Zhu, S., Lou, S., et al., 2022. Elevated formation of particulate nitrate from N_2O_5 hydrolysis in the Yangtze River Delta region from 2011 to 2019. Geophys. Res. Lett. 49.
Zhou, Y., Wang, T., Gao, X., Xue, L.K., Wang, X.F., Wang, Z., et al., 2010. Continuous observations of water-soluble ions in $PM_{2.5}$ at Mount Tai (1534 m a.s.l.) in central-eastern China. J. Atmos. Chem. 64, 107–127.
Zhu, Y., Tilgner, A., Hoffmann, E.H., Herrmann, H., Kawamura, K., Yang, L.X., et al., 2020. Multiphase MCM–CAPRAM modelling of the formation and processing of secondary aerosol constituents observed during the Mt. Tai summer campaign in 2014. Atmos. Chem. Phys. 20, 6725–6747.
Zong, Z., Tian, C., Sun, Z., Tan, Y., Shi, Y., Liu, X., et al., 2022. Long-term evolution of particulate nitrate pollution in North China: isotopic evidence from 10 offshore cruises in the Bohai Sea from 2014 to 2019. J. Geophys. Res. A 127.